Grain Boundary Mapping in Polycrystalline Graphene

Kwanpyo Kim,[†,‡,‖] Zonghoon Lee,[§,⊥,‖] William Regan,[†,‡] C. Kisielowski,[§] M. F. Crommie,[†,‡] and A. Zettl[†,‡,*]

[†]Department of Physics and Center of Integrated Nanomechanical Systems, University of California at Berkeley, Berkeley, California 94720, United States, [‡]Materials Sciences Division, and [§]National Center for Electron Microscopy, Lawrence Berkeley National Laboratory, Berkeley, California 94720, United States, and [⊥]School of Mechanical and Advanced Materials Engineering, Ulsan National Institute of Science and Technology (UNIST), Ulsan 689-798, South Korea.

[‖] These authors contributed equally to this work.

Graphene, with its unusual electrical, mechanical, and thermal properties, presents new opportunities in fundamental research and practical applications.[1−4] Most experimental investigations of graphene have been focused on exfoliated small-area specimens, usually restricted to single-grain regions. Recently, large-area synthesis of high-quality but *polycrystalline* graphene has been advanced as a scalable route to applications including electronic devices.[5−9] The presence of grain boundaries (GBs) may have detrimental effects on some electronic, thermal, and mechanical properties of graphene, including reduced electronic mobility,[6−9] lower thermal conductivity,[10] and reduced ultimate mechanical strength,[11] yet on the other hand, GBs might be beneficially exploited *via* controlled GB engineering.[12] The study of graphene grains and their boundary is therefore critical for a complete understanding of this interesting material and for enabling diverse applications.

Since graphene is a two-dimensional one-atom-thick carbon membrane, the GB in graphene is a one-dimensional entity. This is in contrast to regular three-dimensional materials for which the GB is a two-dimensional surface. The GB of graphite has been investigated using scanning tunneling microscopy (STM) for over 20 years,[13−16] and more recently, STM and other surface studies of grains and boundaries have been performed on epitaxially grown graphene on single-crystal substrates.[17−22] Unfortunately, such surface probe techniques are either extremely time-consuming and not appropriate for large-area characterization[13−18,20−22] or lack suitable spatial resolution in the case of low-energy electron diffraction and

microscopy.[18,19] Moreover, true atomic-resolution imaging at the GB of graphene unperturbed by the substrate structure has not been achieved, hindering fundamental understanding of the electronic and mechanical properties of polycrystalline graphene structures.

TEM, a direct and relatively fast imaging tool ideally suited for suspended atomically thin membranes, has been successfully applied to study adsorbates on graphene using modest-resolution machines[23] and, using aberration-corrected instrumentation, to the local atomic structure of graphene itself.[24−26] We show here that scanning electron diffraction in STEM mode (SED-STEM) makes possible fast and direct identification of GBs. We also demonstrate that dark-field (DF) TEM imaging techniques allow facile GB imaging for high-angle tilt GBs in graphene. GB mapping is systematically carried out on large-area graphene samples *via* these complementary techniques. The study of the detailed atomic structure at a GB in suspended graphene uses aberration-corrected ultra-high-resolution TEM, which shows the theoretically predicted alternating pentagon−heptagon structure along high-angle GBs.

ABSTRACT We report direct mapping of the grains and grain boundaries (GBs) of large-area monolayer polycrystalline graphene sheets, at large (several micrometer) and single-atom length scales. Global grain and GB mapping is performed using electron diffraction in scanning transmission electron microscopy (STEM) or using dark-field imaging in conventional TEM. Additionally, we employ aberration-corrected TEM to extract direct images of the local atomic arrangements of graphene GBs, which reveal the alternating pentagon−heptagon structure along high-angle GBs. Our findings provide a readily adaptable tool for graphene GB studies.

KEYWORDS: graphene · polycrystalline · grain · grain boundary · transmission electron microscopy (TEM)

RESULTS AND DISCUSSION

Graphene was synthesized by adapting a recent report of CVD synthesis on copper foil.[8] After the synthesis, TEM samples were prepared *via* a recently developed direct transfer method.[27] Atomic-resolution TEM imaging, electron diffraction, and Raman spectroscopy analysis confirmed that the graphene from this synthesis method is mostly single layer (see Supporting Information), in agreement with previous reports.[8] STEM images demonstrate that graphene of large area (more than $20\,\mu m \times 20\,\mu m$) can be perfectly transferred to commercial TEM grids, with non-single-layer regions (including local folding structures) comprising less than 10% of the sample area (see Supporting Information).

Grains and GBs are identified using SED-STEM, which involves scanning a nanoparallel electron beam (NPEB) across a suspended graphene membrane in the diffraction mode of STEM. A related diffraction acquisition method with scanning micrometer-size beam has been previously used for domain mapping of polycrystalline films.[28] When the electron beam laterally traverses a tilt GB, gradual transitions are observed from one hexagonal set diffraction to a relatively rotated set (Figure 1); each set results from an individual grain of single-layer graphene. Experimentally obtained graphene diffraction patterns at a transition are shown in Figure 1b–d. Diffraction patterns are acquired with a NPEB of 45 nm diameter. The hexagonal diffraction pattern (A spots) in Figure 1b transitions to a relatively rotated hexagonal pattern (B spots) in Figure 1d. There are intermediate locations in which both hexagonal patterns appear together in a single diffraction graph, as shown in Figure 1c. This occurs when the electron beam simultaneously probes both grains at the interface. Across the transition, the intensity profiles of diffraction A spots show an expected diminishing trend, and those of B spots show an expected intensifying trend, as the area of the associated grain (or number of carbon atoms in its associated graphene grain lattice) under the electron beam illumination, respectively, decreases or increases, as shown in Figure 1e,f.

Intensity variations of A spots, B spots, and their sum across the transition are shown in Figure 1f. Importantly, the intensity sum of A and B spots is nearly constant over the transition. This is compelling evidence that the transition is due to a tilt GB and not another microstructure, such as foldings or overlapping of two misoriented graphene sheets. Compared to single-layer graphene, such overlapping microstructures have multilayer regions and would therefore increase the effective area of crystalline graphene under electron illumination, which would lead to an increase of the intensity sum at a transition, contrary to observations.

The graphene grain's lateral isolation in the sample plane also enables us to perform dark-field (DF) TEM
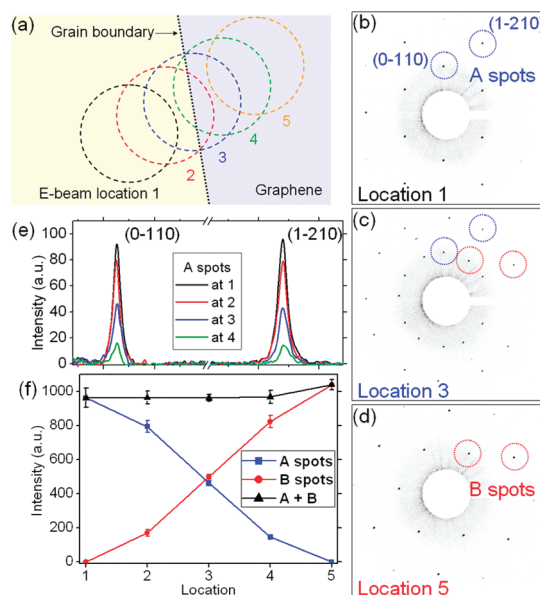

Figure 1. Grain boundary (GB) identification through diffraction series on a graphene sheet. (a) Schematic of GB identification through a series of diffraction pattern acquisitions. The dotted straight line is a tilt GB of graphene dividing the left and right side of the graphene membrane. A series of diffraction acquisitions across a GB will produce a transition from one set of hexagonal diffraction patterns to a relatively rotated set. (b–d) Experimentally obtained diffraction patterns at a transition. Diffraction patterns are acquired with a nanoparallel electron beam of 45 nm diameter. (b) Diffraction pattern showing a set of hexagonal patterns from single-layer graphene. (c) Diffraction pattern showing two sets of the hexagonal pattern, which are relatively rotated by 26.0°. (d) Diffraction pattern with a different hexagonal pattern after the completion of a transition. (e) Intensity profiles of diffraction A spots across the transition. The left and right peaks are the intensity profiles for (0−110) and (1−210) spots. (f) Intensity variations of A spots, B spots, and their sum across the transition.

imaging for facile GB identification in the case of highly rotated (>~10°) tilt GBs. Figure 2a shows a bright-field (BF) TEM image of graphene (prepared on a commercial Quantifoil holey carbon grid) where a diffraction transition occurs. There are no special features that appear to be GBs in the BF image. Figure 2b shows a diffraction pattern with two sets of hexagonal patterns at the transition, which are relatively rotated by 25.6°. We selectively obtain the bright contrast enhancement in one grain by transmitting only a single diffraction spot (marked with dotted circles c or d) with a small objective aperture. Figure 2c clearly reveals that the left side is brighter than the right side of the DF image, which is divided by a sharp line feature. The illumination change to the other transmitted diffraction spot produces a DF image with the inverted contrast in the graphene area (Figure 2d), while the line feature does not change. There is no overlap between the two bright regions in the two DF images (Figure 2c,d). This demonstrates that the line feature thus identified is a GB, not a local overlapping of two distinct graphene
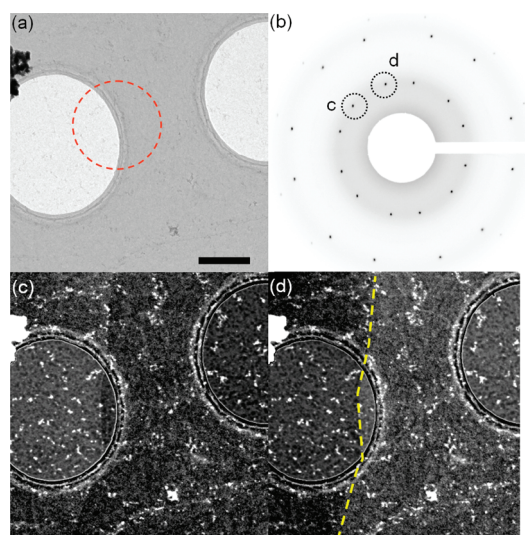
Figure 2. Imaging of a graphene GB *via* TEM dark-field imaging. (a) TEM bright-field image of graphene on a commercial TEM grid (Quantifoil holey carbon) at a diffraction transition. The red dashed circle is the field of view for the diffraction pattern acquisition for panel b. The scale bar is 500 nm. (b) Diffraction pattern with two sets of the hexagonal pattern, showing a 25.6° misorientation. Diffraction spots circled by dashed lines c and d are transmitted for dark-field imaging, respectively, for panels c and d. Amorphous carbon of the TEM grid contributes the halo pattern to the diffraction pattern. (c) Dark-field (DF) TEM image of the same area from the (0−110) diffraction spot. The left side is brighter than the right side of the image, separated by a line (the GB). (d) DF TEM image with (0−110) spot d from the other set of hexagonal diffraction spots shows the inverted contrast in the graphene area. For panels c and d, the brightness is adjusted separately between inside and outside of the amorphous carbon holes. The yellow dashed line is a guide to the eye for the graphene GB.

structures. We note that the GB is generally straight but changes its direction locally along the boundary in this magnification range.

We have used both SED-STEM and DF-TEM to map out graphene grains and their boundaries over a scale large enough to encompass multiple grains. In a precollected SED-STEM image, we mark and compile the locations where diffraction patterns make transitions for tracing a grain map. The DF technique can confirm this mapping process at high-angle GBs. Figure 3a shows a graphene GB map overlaid on the corresponding STEM image. The annotated angles inside the grains are the relative angles of the grain's hexagonal diffraction pattern measured against a reference grain (overlaid in red) at the central region. We determine a graphene grain size in the range of 3−10 μm using our synthesis conditions. One should caution that identified grain boundaries in this study are restricted to the cases of tilt GBs. Even though nontilted GBs can exist in graphene,[21] SED-STEM and DF-TEM methods are only applicable for visualizing tilt GBs in graphene. Aberration-corrected TEMs, which will be discussed later in this article, can be utilized to image nontilted GBs.
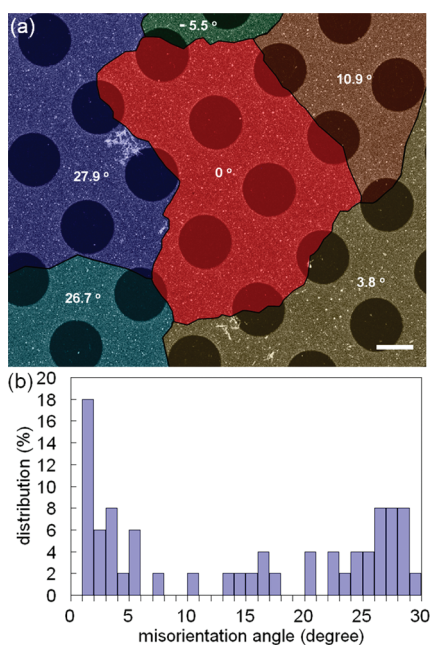

Figure 3. Graphene GB mapping. (a) GB map with an overlaid background of the graphene STEM image. The annotated angles inside each grain are the relative angles of the hexagonal diffraction pattern measured against the grain at the center. The grain mapping was performed mainly using a nanoparallel electron beam of size ~45 nm in STEM mode. The scale bar is 1 μm. (b) Distribution of misorientation angles between adjacent grains. Fifty misorientation angles are measured from rotational angles between two sets of hexagonal diffraction patterns. There are more populations around 0 and 30° than middle-range angles.

Macroscopic mapping of graphene GBs additionally allows us to systematically investigate the relative misorientation angles between adjacent grains (Figure 3b). A misorientation angle can be defined to be smaller than 30° in our study due to the hexagonal symmetry. It is found that significant portions of misorientations are located around 0° (low-angle tilt GB) and 30° (high-angle). The reported grain size of the polycrystalline copper used for our graphene synthesis is approximately 100 μm,[7] which is much bigger than the graphene grain size we have found here. Hence, numerous graphene GB formations occur within a single copper grain. The high percentage of 0° and 30° misorientations implies that there are interactions from the copper substrate causing the preferential lattice alignment of graphene during the graphene synthesis. A related study correlating preferential growth directions of graphene with the crystalline direction of the underlying Cu(111) substrate has been recently reported.[22] Further systematic study of graphene synthesis on single-crystal and polycrystalline copper will help in understanding graphene growth and substrate alignment.

Aberration-corrected TEMs have been used to image atomic defects on carbon nanotubes and graphene including vacancies and topological defects.[24−26] Recently, there has been a report of GB-like structures in
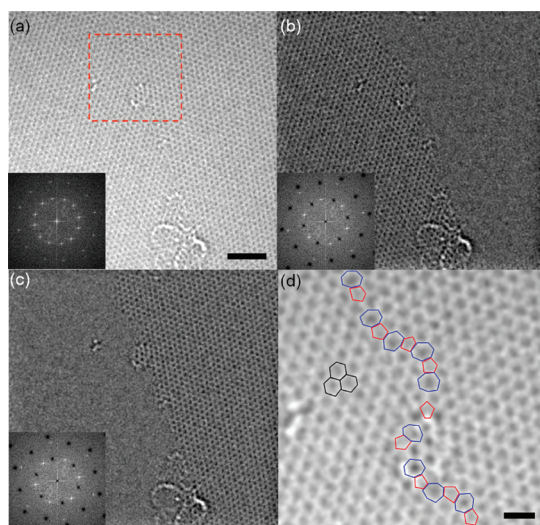
Figure 4. Atomic-resolution images of a high-angle tilt GB of graphene. (a) Atomic-resolution image of graphene GB. The left and right parts of the image are different tilt grains, which are relatively tilted by 26.6°. The red dashed rectangle is the field of view for panel d. The inset shows the Fourier transform of the image. It shows the two sets of hexagonal patterns from two grains. The scale bar is 2 nm. (b) Atomic-resolution image of the same region after removing one set of hexagonal patterns from the fast Fourier transform. The contrast of the right side of the image completely disappears, indicating that the graphene has no defects inside the right side grain. (c) Atomic-resolution image after removing another set of hexagonal patterns from the fast Fourier transform. The left side of the image disappears. (d) Zoom-in image of the high-angle tilt GB of graphene. The pentagon, hexagon, and heptagon are overlaid with red, black, and blue polygons, respectively. The GB shows an array of alternating pentagon and heptagon structures. The scale bar is 0.5 nm.

few-layer graphene, but the atomic structure could not be clearly resolved due to multilayer interference.[29] Copper-catalyzed CVD graphene is ideal for atomic-resolution GB imaging as it is mainly single layer and offers large sample areas with multiple GBs. We have investigated suspended CVD-grown graphene in the TEAM 0.5 aberration-corrected microscope. We start by scanning a graphene sample while monitoring its diffraction pattern. When the diffraction pattern shows a transition of the diffraction angle, we stop moving the sample stage and perform atomic-resolution imaging at the transition region.

Figure 4 confirms that tilt GBs are the origin of the diffraction transitions we have observed. Figure 4a shows an atomic-resolution image of a high-angle tilt GB of single-layer graphene, which is acquired using

image Cs aberration correction with a monochromated beam at 80 keV. The left and right parts of the image are two different grains, which are relatively tilted by 26.6°. The inset shows the Fourier transform of the image and reveals the two sets of hexagonal patterns from two individual grains. After removing one hexagonal pattern set and performing inverse Fourier transforms, we easily distinguish the distinct graphene grains (Figure 4b,c). In Figure 4b, the contrast of the right side of the image completely disappears, indicating that the graphene has no defects inside the grain.

The zoomed-in image of Figure 4d reveals the detailed atomic structure of a high-angle GB of graphene. Pentagons, hexagons, and heptagons, defined by individual carbon atom positions, are overlaid with red, black, and blue polygons, respectively. It is clear that this high-angle GB consists of an array of alternating pentagons and heptagons without other defect structures such as vacancies, similar to theoretical predictions of graphene high-angle GBs.[11,30,31] The pentagon−heptagon GB is fairly stable under the electron beam, proving its mechanical integrity. The GB exhibits a mixture of different types of dislocations with Burgers vectors of (1,0) and (1,1).[11,30,31] The GB also shows local bending at the atomic scale; the majorities of GB segments are found to deviate from the symmetric bisecting line, a result not accounted for in simple theoretical models.[11,30,31] Of course, details of the GB structure may be sensitive to graphene synthesis conditions.

CONCLUSIONS

In conclusion, we present a study of tilt GBs of large-area monolayer polycrystalline graphene using complementary TEM techniques. Conventional-resolution TEM yields structural identification of grains and their boundaries in suspended graphene samples if SED-STEM or DF-TEM modes are employed. The presented methods can readily be used to assess the quality of polycrystalline graphene samples and aid in engineering GBs to exploit their peculiar electronic properties.[12] Moreover, we present the atomic-resolution imaging of high-angle tilt GBs in graphene membranes. Our findings will likely benefit future theoretical and experimental studies on thin membrane grains and GBs, including boundary diffusion, electronic structure modification, and possible enhanced chemical reactivity at the boundary.

METHODS

Graphene Sample Preparation. Graphene is synthesized on 25 μm thick copper foil (99.8% Alfa Aesar, Ward Hill, Ma), following a recent report.[8] After the synthesis, graphene is transferred to Quantifoil holey carbon TEM grids using a direct transfer method.[27] In brief, we place the Quantifoil TEM grid onto a graphene-covered copper foil such that the Quantifoil

carbon film side faces the graphene. Then we wet the sample with a drop of isopropyl alcohol and dry it with a home-built vacuum line to promote adhesion between the Quantifoil carbon film and the graphene. Heating the sample at 120 °C on a hot plate can produce better adhesion. The sample is placed into a solution of $FeCl_3$ to etch the underlying copper foil and is then rinsed in deionized water. Before putting TEM

samples into the microscope, the sample is heated at 180 °C for 10 min to remove adsorbates on the graphene surface.

Diffraction Acquisition and Imaging. We use a Zeiss Libra 200F operated at 200 keV. The microscope optics use the nanoparallel electron beam (NPEB) setup optimized for fine diffraction pattern acquisition in STEM mode. In our work, we use two different configurations which give nanoparallel circular beams with diameters of 830 and 45 nm, respectively. The 45 nm beam is used for Figure 1 and Figure 3 grain mapping. The 830 nm beam is used for diffraction data in Figure 2 and Figure 3. All diffraction patterns are energy filtered with 40 eV width. Bright-field and dark-field TEM imaging is also performed using the same microscope in TEM imaging mode.

Aberration-Corrected TEM. TEAM 0.5, operated at 80 keV, is used for atomic-resolution imaging of graphene grain boundaries. The low acceleration voltage minimizes the electron beam damage to the graphene samples. The microscope is tuned by the image Cs aberration corrector with a monochromated beam giving a spatial resolution of better than 1 Å, which enables us to resolve individual carbon atoms at the grain boundaries.

Supporting Information Available: Additional figures for characterization of single-layer CVD graphene samples, additional atomic-resolution TEM images of a tilt grain boundary, and a movie (real-time video recording) of graphene diffraction pattern transitions through grain boundaries in graphene. This material is available free of charge *via* the Internet at http://pubs.acs.org.

REFERENCES AND NOTES

1. Geim, A. K.; Novoselov, K. S. The Rise of Graphene. *Nat. Mater.* **2007,** *6*, 183–191.
2. Castro Neto, A. H.; Guinea, F.; Peres, N. M. R.; Novoselov, K. S.; Geim, A. K. The Electronic Properties of Graphene. *Rev. Mod. Phys.* **2009,** *81*, 109–162.
3. Lee, C.; Wei, X.; Kysar, J. W.; Hone, J. Measurement of the Elastic Properties and Intrinsic Strength of Monolayer Graphene. *Science* **2008,** *321*, 385–388.
4. Baladin, A. A.; Ghosh, S.; Bao, W.; Calizo, I.; Teweldebrhan, D.; Miao, F.; Lau, C. N. Superior Thermal Conductivity of Single-Layer Graphene. *Nano Lett.* **2008,** *8*, 902–907.
5. Berger, C.; Song, Z.; Li, T.; Li, X.; Ogbazghi, A. Y.; Feng, R.; Dai, Z.; Marchenkov, A. N.; Conrad, E. H.; First, P. N.; de Heer, W. A. Ultrathin Epitaxial Graphite: 2D Electron Gas Properties and a Route toward Graphene-Based Nanoelectronics. *J. Phys. Chem. B* **2004,** *108*, 19912–19916.
6. Kim, K. S.; Zhao, Y.; Jang, H.; Lee, S. Y.; Kim, J. M.; Kim, K. S.; Ahn, J. H.; Kim, P.; Choi, J. Y.; Hong, B. H. Large-Scale Pattern Growth of Graphene Films for Stretchable Transparent Electrodes. *Nature* **2009,** *457*, 706–710.
7. Reina, A.; Jia, X.; Ho, J.; Nezich, D.; Son, H.; Bulovic, V.; Dresselhaus, M. S.; Kong, J. Large Area, Few-Layer Graphene Films on Arbitrary Substrates by Chemical Vapor Deposition. *Nano Lett.* **2009,** *9*, 30–35.
8. Li, X.; Cai, W.; An, J.; Kim, S.; Nah, J.; Yang, D.; Piner, R.; Velamakanni, A.; Jung, I.; Tutuc, E.; *et al.* Large-Area Synthesis of High-Quality and Uniform Graphene Films on Copper Foils. *Science* **2009,** *324*, 1312–1314.
9. Bae, S.; Kim, H. K.; Lee, Y.; Xu, X.; Park, J. S.; Zheng, Y.; Balakrishnan, J.; Lei, T.; Kim, H. R.; Song, Y. I.; *et al.* Roll-to-Roll Production of 30-Inch Graphene Films for Transparent Electrodes. *Nat. Nanotechnol.* **2010,** *5*, 574–578.
10. Cai, W.; Moore, A. L.; Zhu, Y.; Li, X.; Chen, S.; Shi, L.; Ruoff, R. S. Thermal Transport in Suspended and Supported Monolayer Graphene Grown by Chemical Vapor Deposition. *Nano Lett.* **2010,** *10*, 1645–1651.
11. Grantab, R.; Shenoy, V. B.; Ruoff, R. S. Anomalous Strength Characteristics of Tilt Grain Boundaries in Graphene. *Science* **2010,** *330*, 946–948.
12. Yazyev, O. V.; Louie, S. G. Electronic Transport in Polycrystalline Graphene. *Nat. Mater.* **2010,** *9*, 806–809.
13. Albrecht, T. R.; Mizes, H. A.; Nogami, J.; Park, S. I.; Quate, C. F. Observation of Tilt Boundaries in Graphite by Scanning Tunneling Microscopy and Associated Multiple Tip Effects. *Appl. Phys. Lett.* **1988,** *52*, 362–364.
14. Simonis, P.; Goffaux, C.; Thiry, P. A.; Biro, L. P.; Lambin, Ph.; Meunier, V. STM Study of a Grain Boundary in Graphite. *Surf. Sci.* **2002,** *511*, 319–322.
15. Pong, W. T.; Bendall, J.; Burkan, C. Observation and Investigation of Graphite Superlattice Boundaries by Scanning Tunneling Microscopy. *Surf. Sci.* **2007,** *601*, 498–509.
16. Červenka, J.; Flipse, C. F. J. Structural and Electronic Properties of Grain Boundaries in Graphite: Planes of Periodically Distributed Point Defects. *Phys. Rev. B* **2009,** *79*, 195429.
17. Coraux, J.; N'Diaye, A. T.; Busse, C.; Michely, T. Structural Coherency of Graphene on Ir(111). *Nano Lett.* **2008,** *8*, 565–570.
18. Loginova, E.; Nie, S.; Thürmer, K.; Bartelt, N. C.; McCarty, K. F. Defects of Graphene on Ir(111): Rotational Domains and Ridges. *Phys. Rev. B* **2009,** *80*, 085430.
19. Sutter, P. W.; Flege, J. I.; Sutter, E. A. Epitaxial Graphene on Ruthenium. *Nat. Mater.* **2008,** *7*, 406–411.
20. Varchon, F.; Mallet, P.; Magaud, L.; Veuillen, J. Y. Rotational Disorder in Few-Layer Graphene Films on 6*H*-SiC(000−1): A Scanning Tunneling Microscopy Study. *Phys. Rev. B* **2008,** *77*, 165415.
21. Lahiri, J.; Lin, Y.; Bozkurt, P.; Oleynik, I. I.; Batzill, M. An Extended Defect in Graphene as a Metallic Wire. *Nat. Nanotechnol.* **2010,** *5*, 326–329.
22. Gao, L.; Guest, J. R.; Guisinger, N. P. Epitaxial Graphene on Cu(111). *Nano Lett.* **2010,** *10*, 3512–3516.
23. Meyer, J. C.; Girit, C. O.; Crommie, M. F.; Zettl, A. Imaging and Dynamics of Light Atoms and Molecules on Graphene. *Nature* **2008,** *454*, 319–322.
24. Hashimoto, A.; Suenaga, K.; Gloter, A.; Urita, K.; Iijima, S. Direct Evidence for Atomic Defects in Graphene Layers. *Nature* **2004,** *430*, 870–873.
25. Suenaga, K.; Wakabayashi, H.; Koshino, M.; Sato, Y.; Urita, K.; Iijima, S. Imaging Active Topological Defects in Carbon Nanotubes. *Nat. Nanotechnol.* **2007,** *2*, 358–360.
26. Meyer, J. C.; Kisielowski, C.; Erni, R.; Rossell, M. D.; Crommie, M. F.; Zettl, A. Direct Imaging of Lattice Atoms and Topological Defects in Graphene Membranes. *Nano Lett.* **2008,** *8*, 3582–3586.
27. Regan, W.; Alem, N.; Alemán, B.; Geng, B.; Girit, C.; Maserati, L.; Wang, F.; Crommie, M.; Zettl, A. A Direct Transfer of Layer-Area Graphene. *Appl. Phys. Lett.* **2010,** *96*, 113102.
28. Sinitskii, A.; Abramova, V.; Laptinskaya, T.; Tretyakov, Y. D. Domain Mapping of Inverse Photonic Crystals by Laser Diffraction. *Phys. Lett. A* **2007,** *366*, 516–522.
29. Park, H. J.; Meyer, J.; Roth, S.; Skákalová, V. Growth and Properties of Few-Layer Graphene Prepared by Chemical Vapor Deposition. *Carbon* **2010,** *48*, 1088–1094.
30. Yazyev, O. V.; Louie, S. G. Topological Defects in Graphene: Dislocations and Grain Boundaries. *Phys. Rev. B* **2010,** *81*, 195420.
31. Liu, Y.; Yakobson, B. I. Cones, Pringles, and Grain Boundary Landscapes in Graphene Topology. *Nano Lett.* **2010,** *10*, 2178–2183.